Research article

Intravoxel incoherent motion diffusion-weighted imaging for oropharyngeal squamous cell carcinoma: Correlation with human papillomavirus Status

Antonello Vidiri[a], Simona Marzi[b,*], Emma Gangemi[a], Maria Benevolo[c], Francesca Rollo[c], Alessia Farneti[d], Laura Marucci[d], Filomena Spasiano[d], Francesca Sperati[e], Francesca Di Giuliano[a,f], Raul Pellini[g], Giuseppe Sanguineti[d]

[a] Radiology and Diagnostic Imaging Department, IRCCS Regina Elena National Cancer Institute, Via Elio Chianesi 53, 00144, Rome, Italy
[b] Medical Physics Laboratory, IRCCS Regina Elena National Cancer Institute, Via Elio Chianesi 53, 00144, Rome, Italy
[c] Department of Pathology, IRCCS Regina Elena National Cancer Institute, Via Elio Chianesi 53, 00144, Rome, Italy
[d] Department of Radiotherapy, IRCCS Regina Elena National Cancer Institute, Via Elio Chianesi 53, 00144 Rome, Italy
[e] Biostatistics-Scientific Direction, IRCCS Regina Elena National Cancer Institute, Via Elio Chianesi 53, 00144, Rome, Italy
[f] Department of Biomedicine and Prevention, University of Rome "Tor Vergata", Viale Oxford 81, 00133, Rome, Italy
[g] Department of Otolaryngology & Head and Neck Surgery, Regina Elena National Cancer Institute, Via Elio Chianesi 53, 00144, Rome, Italy

ARTICLE INFO

ABSTRACT

Purpose: To investigate the relationships between imaging parameters derived from intravoxel incoherent motion diffusion-weighted imaging (IVIM-DWI) and HPV status in oropharyngeal squamous cell carcinoma (OPSCC).

Materials and Methods: 73 patients with a new diagnosis of OPSCC were enrolled in the present study. MRI including IVIM-DWI with nine b value (range 0–800 s/mm^2) was acquired in all patients. Primary tumor (PT) and the largest metastatic lymph node (LN), if present, were volumetrically contoured and the tissue diffusion coefficient D_t, perfusion fraction f and perfusion-related diffusion coefficient D^* were estimated by a bi-exponential fit. The apparent diffusion coefficient (ADC) was also estimated by a mono-exponential fit. The predictive power of the most relevant patient/tumor characteristics and image-based features in determining the HPV status was assessed.

Results: 67 PTs and 67 metastatic LNs were analyzed. Significant differences in ADC and D_t values among HPV-positive and HPV-negative patients were found for PTs (p = 0.003 and p < 0.001, respectively), while a trend toward significance in D_t was reported for LNs (p = 0.066). The perfusion-related parameters, f, D^* and $D^* \times f$, were not related to HPV status. The best predictive model for HPV positivity was obtained combining alcohol intake and smoke habits with D_t values of PTs (accuracy = 80.8%, sensitivity = 85.7%, specificity = 64.7%).

Conclusion: Significant correlations were found between IVIM-DWI and HPV status in OPSCCs. The perfusion-free diffusion coefficient, D_t, may better reflect the HPV-related tumor differences compared to ADC, whereas the perfusion-related parameters were not able to reliably discriminate HPV-positive from HPV-negative OPSCC.

1. Introduction

During the last few decades, there has been an increase in the incidence of oropharyngeal squamous cell carcinoma (OPSCC) related to the human papilloma virus (HPV) infection [1].

Currently, HPV-related OPSCC is recognized as a distinct subtype of head and neck squamous cell carcinoma (HNSCC) with unique molecular pathogenesis, demographic profile, clinical presentation and prognosis [2]. In many reports, HPV status portends a better prognosis and is recognized as an important independent prognostic factor for OPSCC [3,4]. To provide a more accurate prediction of survival for newly diagnosed patients, the recently released 8th edition of American Joint Committee on Cancer (AJCC) staging manual, head and neck section, has separated the staging algorithm for HPV-positive OPSCC from that of HPV-negative ones [5].

In the last few years, several studies have reported differences in imaging characteristics of OPSCC by HPV status at Computed Tomography (CT) [6–9], Magnetic Resonance (MR) [8,10–14], Positron

---

Emission Tomography (PET) [15,16] or a combination of multimodality imaging techniques [17,18].

On MR morphological sequences, HPV-positive OPSCCs often present as small primary tumors with defined borders and exophytic appearance, while lymph node metastases are more frequently cystic. In contrast, HPV-negative OPSCCs appear as bulky primary tumors with irregular borders, ulceration and necrosis, and lymph node metastases show a similar topographic distribution [19].

Besides conventional anatomic images, there is a rising trend toward additional functional MR imaging, such as diffusion-weighted imaging (DWI), for further characterization of tissues. In previous studies, HPV-positive tumors have been associated to lower apparent diffusion coefficient (ADC) values at DWI compared to HPV-negative ones [10,12,13,18]. Interestingly, other studies have shown that ADC is able to discriminate squamous cell carcinomas of the head and neck likely to respond to chemo-radiotherapy, with those with lower ADC values showing a more favorable outcome [20–22].

However, it has been recognized that the interpretation of ADC may be difficult, as it represents a global parameter which may be affected by complex biophysical processes occurring on a macroscopic voxel scale, related to tissue cellularity and organization, extracellular space tortuosity and microcapillary perfusion [23]. To account for the effects of microcapillary perfusion on DWI measurements [24], a specialized imaging technique, known as intravoxel incoherent motion (IVIM) imaging, was proposed, which provide quantitative parameters that separately reflect tissue diffusivity and tissue microcapillary perfusion [23].

Several diagnostic and prognostic studies have previously investigated the potential of IVIM-DWI in HN cancer patients [25] and it concordantly emerged that IVIM-DWI may be useful for characterizing and differentiating between benign and malignant pathologies [26], early evaluating the treatment response to therapy and assessing residual /recurrent disease [27–29].

We hypothesize that IVIM-DWI may also provide a clearer interpretation of the differences in diffusion parameters of OPSCC by HPV status, allowing to investigate also the role of tumor vascularity through perfusion-related diffusion parameters.

In January 2016 we started a prospective study funded by the Italian Association for Cancer Research (AIRC, project No. 17028) in locally advanced OPSCC, to investigate the ability of IVIM-DWI to predict tumor response to chemo-radiotherapy. As part of this ongoing study, we investigated the relationship between pre-treatment IVIM-DWI parameters and HPV status, along with selected patient- and tumor-related factors.

2. Materials and methods

2.1. Patient population

To be enrolled in the present prospective study, patients had to fulfill all the following criteria: (i) age older than 18 years; (ii) Karnofsky performance status > 80; (iii) pathologically confirmed squamous cell carcinoma of the oropharynx; (iv) stage III or IV without distant metastases according to the 8th edition of American Joint Committee on Cancer (AJCC) staging system; (v) treatment with radiotherapy $\pm$ chemotherapy. Exclusion criteria included: any contraindication to MR examination; prior surgery, CHT (including induction chemotherapy) or radiotherapy to the primary disease and the neck. Moreover, specific informed consent was obtained from each patient. The study protocol was authorized by the local Institutional Review Board.

Demographic data of the enrolled patients were obtained and tumor subsites, cigarette smoking and alcohol consumption were recorded.

2.2. HPV testing

Both p16 immunohistochemistry and PCR-based detection techniques were used to identify HPV-positive OCSCC. HPV-positive patients were defined as those with both p16-positive and HPV-DNA positive tumors [30].

For each formalin-fixed paraffin-embedded (FFPE) cancer tissue 1–3 x 5 μm sections were cut, the number of sections depending on the tissue size. DNA was purified using the DNeasy Blood and Tissue Kit (Qiagen). The PCR-based INNO-LiPA HPV Genotyping *Extra* II kit (Fujirebio) and TENDIGO™ instrument (Fujirebio) were used for HPV-DNA detection and genotyping. This assay identifies 32 High risk and low risk HPV types.

The CINtec® Histology Kit (Roche Diagnostics, Milan, Italy) was used to assess the expression of p16 protein following the manufacturer's instructions. The staining was evaluated according to AJCC Cancer Staging Manual [5]. More details are given in Supplementary Materials.

2.3. MR imaging protocol

MRI was performed on a 1.5-T system (Optima MR 450 w, GEHealth-care, Milwaukee, WI, USA) with dedicated 16-channel receive only radiofrequency coils: a head coil, a surface neck coil, and a spine coil.

The MRI examination included fast spin-eco (FSE) T2-weighted images on the coronal plane (acquisition matrix 288 × 256, field of view 27 x 27 cm, TR/TE 5901 ms/102; slice thickness 4 mm), followed by axial FSE T2-weighted images (acquisition matrix 288 × 256, field of view 26–28 cm, TR/TE 6844 ms/105; slice thickness 3 mm), and pre-contrast T1-weighted images (acquisition matrix 288 × 256, field of view 26–28 cm, TR/TE 617 ms/8.1; slice thickness 3 mm,) on the axial plane, acquired from the level of the skull base to the thoracic inlet.

DWI were obtained via single-shot spin-echo and echo-planar imaging (acquisition matrix, 128 × 128; field of view, 26–28 cm; TR/TE 4500 ms/77 ms; slice thickness 4 mm; spacing between slices 5 mm, bandwidth 1953 Hz/pixel). Nine different b values (b = 0, 25, 50, 75, 100, 150, 300, 500 and 800 s/mm^2) were used, with the diffusion-sensitizing gradients applied in three orthogonal directions to obtain trace-weighted images.

Three signal averages were used for b values ranging from 0 to 300 s/mm^2, four for b values of 500 s/mm^2, and five for b values of 800 s/mm^2. A scan time reduction factor of two was used, with a resulting scan duration of 6 min and 13 s.

The imaging protocol also included post-contrast (Gadolinium 0,1 mmol/kg) T1-weighted images with Liver Acquisition with Volume Acceleration sequences (LAVA; acquisition matrix 288 × 288, field of view 26-28 cm, TR/TE 9.8 ms/min; slice thickness 1 mm, 214 slices), in axial and coronal planes, as required for the routine examination.

2.4. Tumor delineation

The volumes of primary tumor (PT) and the largest metastatic lymph node (LN) were identified and manually contoured on DWI with b = 800 s/mm^2 by two expert HN radiologists (A.V. and E.G.) in consensus. Morphological T2-weighted images and/or post-contrast T1-weighted images were used as a guide for tumor delineation. All lesion-containing sections were outlined, including necrosis, while arterial or venous structures, and bony components were excluded from the volumes of interest (VOIs). The volume size of each PT and LN was also quantified on morphological images and recorded. The 3D Slicer Software (Version 4.1.1) was used for visualizing the image sets and for the lesion segmentation.

The LNs were classified as solid, cystic or necrotic, based on their morphologic characteristics evaluated on T2-weighted imaging and/or post-contrast T1-weighted images [31]. More details are given in

Table 1
Patient and tumor characteristics sorted by human papillomavirus (HPV) status.

Patient and tumor characteristics		HPV-negative (n = 19)	HPV-positive (n = 54)	Chi2 p
		n(%)	n(%)	
Gender	*Male*	18 (30.5)	41 (69.5)	0.096
	Female	1 (7.1)	13 (92.9)	
Age (mean ± SD)		65.4 ± 9.1	61.7 ± 9.5	0.140
Tumour site	*Tonsil*	8 (20.0)	32 (80.0)	0.322
	Base of the tongue	11 (34.4)	21 (65.6)	
	Both	0 (0.0)	1 (100.0)	
T-stage	*T1-2*	7 (24.1)	22 (75.9)	0.765
	T3-4	12 (27.3)	32 (72.7)	
N-stage	*N0*	3 (60.0)	2 (40.0)	< **0.001**
	N1	1 (3.0)	32 (97.0)	
	N2-3	15 (42.9)	20 (57.1)	
Smoking status	*0-5pack/yr*	3 (10.3)	26 (89.7)	**0.003**
	6-24pack/yr	1 (9.1)	10 (90.9)	
	> 24pack/yr	15 (45.5)	18 (54.5)	
Alcohol intake	*No*	6 (13.0)	40 (87.0)	< **0.001**
	Moderate	3 (21.4)	11 (78.6)	
	Heavy	10 (76.9)	3 (23.1)	
Nodal Morphology	*Solid*	9 (23.7)	29 (76.3)	0.996
	Cystic	1 (25)	3 (75)	
	Necrotic	6 (23.1)	20 (76.9)	

Statistically significant p-values are bold.

Supplementary Materials.

2.5. Calculation of IVIM-diffusion parameters

The delineated contours were loaded into a MATLAB workspace (Release R2017b, The Mathworks Inc., Natick, Massachusetts), where dedicated scripts were developed for the quantitative image analyses. The median value of the signal from all voxels within the delineated volume (PT or LN) was derived for each b value and its variation at increasing b was modeled using the following bi-exponential function [23]:

$$S_b/S_0 = (1-f)\cdot e^{-b\cdot D_t} + f\cdot e^{-b\cdot(D_t + D^*)} \tag{1}$$

where S_b is the signal intensity with diffusion weighting b, S_0 is the signal intensity for a b value of 0 s/mm^2, f is the fractional volume of capillary blood, D_t is the tissue diffusion coefficient (in mm^2/s), and D* is the perfusion-related diffusion coefficient (in mm^2/s). The parameters were determined according to Eq.1, by a nonlinear constrained minimization algorithm [32], as described elsewhere [29]. More details are given in Supplementary Materials.

The product of D* by *f* was also derived, as a linear relationship has been supposed between this product and blood flow in the brain [33].

The conventional ADC was calculated from data at *b* values of 0, 500 and 800 s/mm^2, using a mono-exponential model. The Levenberg-Marquardt algorithm was used to perform the mono-exponential fits of both D_t and ADC.

2.6. Statistical analyses

Continuous data were reported as median values and interquartile ranges and the categorical data with frequencies and percentage values. Kolmogorov-Smirnov test was applied in order to evaluate the normality distribution of the data. We explored the differences between continuous variables, performing the Student's *t*-test or the Mann-Whitney test, depending on the distribution of the data. The relationships between categorical variables were evaluated using Chi2 or Fisher's Exact test, as appropriate. The Wilcoxon test for paired data was used to compare the imaging parameters, sorted by HPV status, while the non-parametric Spearman rank correlation test was applied to assess the correlations.

Further analyses were performed by dividing the patient population into three subgroups of patients: HPV-negative patients, HPV-positive nonsmoker (< 5 pack/yr) nonalcoholic patients and HPV-positive smoker (≥6 pack/yr) and moderate or heavy alcoholic patients. Patients were defined as moderate alcoholic if they drunk < 1 L of wine/day and heavy alcoholic if they drunk ≥1 L of wine/day. To evaluate potential differences between these patient groups, we performed the Kruskall-Wallis Test or Chi2, when appropriate. We also applied the Bonferroni's correction in order to reduce the probability of significant differences due to multiple testing. The statistical calculations were performed using SPSS statistical software version 21 (SPSS inc., Chicago IL, USA).

A *Decision Tree* classification learner [34] was used to assess the predictive power of the most relevant patient/tumor characteristics and image-based features in determining the HPV-related OPSCC. A data cross-validation (5 fold) was applied to avoid overfitting due to the small data set. The found classification performance was reported in terms of Accuracy, Sensitivity, Specificity, Positive Predictive Value (PPV), Negative Predictive Value (NPV). The Matlab code (Release R2017b, The Mathworks Inc., Natick, Massachusetts) was used to perform this analysis.

To support the *Decision Tree* prediction model, an univariate logistic regression model was also applied. Then, a multivariate logistic regression model was used with predictive variables that were significant in the univariate analyses following the forward selection method.

3. Results

3.1. Patient population

A total of 73 patients affected by OPSCC were prospectively enrolled in the present study from January 2016 to June 2018. Patient and tumor characteristics are summarized in Table 1. Fifty four patients were HPV-positive and 19 HPV-negative. Patients with HPV-related OPSCC tended to be younger (p = 0.14), smoked and drunk less (p = 0.003 and p < 0.001, respectively) and were more likely to have a higher N-stage (p < 0.001) than patients with non HPV-related OPSCC. No significant difference was found in terms of LN morphology (solid/cystic/necrotic) between the two groups of patients.

Table 2

Summary statistics of IVIM-DWI parameters and volume size in primary tumors (PTs) and metastatic lymph nodes (LNs) sorted by human papillomavirus (HPV) status.

Parameter*	PTs (n = 67)			LNs (n = 67)		
	HPV-negative (n = 17)	HPV-positive (n = 50)	p	HPV-negative (n = 15)	HPV-positive (n = 52)	p
ADC(10^{-3} mm^2/s)	1.58 (1.33-1.83)	1.27 (1.06-1.47)	**0.003**	1.34 (1.02-1.47)	1.13 (0.99-1.27)	0.097
D_t(10^{-3} mm^2/s)	1.20 (1.03-1.36)	0.97 (0.83-1.06)	**< 0.001**	1.11 (0.87-1.22)	0.91 (0.81-1.08)	0.066
f (%)	15.57 (8.65-29.52)	13.28 (10.24-18.89)	0.538	11.32 (7.52-15.01)	8.53 (6.98-11.80)	0.247
D*(10^{-3} mm^2/s)	16.87 (6.88-38.13)	19.21 (14.20-40.92)	0.319	16.75 (9.54-26.20)	20.97 (12.43-53.99)	0.223
D* × f (10^{-3} mm^2/s)	0.23 (0.12-0.40)	0.27 (0.18-0.46)	0.342	0.13 (0.09-0.28)	0.20 (0.09-0.31)	0.537
Volume (cm^3)	15.31 (7.67-32.12)	11.30 (6.10-22.10)	0.356	4.25 (1.69-8.30)	5.75 (2.45-15.32)	0.588

Median values (Interquartile range)*. P values refer to Mann-Whitney test. Statistically significant p-values are bold. Abbreviations: ADC, apparent diffusion coefficient; D_t, tissue diffusion coefficient; D*, perfusion-related diffusion coefficient; f(%), perfusion fraction; D* × f, product of D* by f.

3.2. Analysis of IVIM-DWI parameters and ADC

In five patients, the IVIM-DWI analysis of PTs was not possible due to the too small volume sizes (< 1 cm^3); one patient was excluded due to the poor image quality as a result of susceptibility and motion artifacts; five patients had no metastatic lymph nodes. Therefore, 67 PTs (17 HPV-negative and 50 HPV-positive) and 67 metastatic LNs (15 HPV-negative and 52 HPV-positive) were analyzed.

Significant differences in both mean ADC and D_t values between HPV-positive and HPV-negative patients were found for PTs (p = 0.003 and p < 0.001, respectively), while a trend toward significance in mean D_t was reported for LNs (p = 0.066). The perfusion-related parameters, f, D* and D* × f were not found to be different by HPV status for both PTs and LNs. No statistically significant differences in the volumes of PTs and LNs were observed on the basis of HPV status (Table 2).

Statistically significant difference in D_t between HPV-negative and HPV-positive patients was found in PTs, regardless of smoking and drinking habit (Supplementary Table 1), while no difference emerged in LNs (Supplementary Table 2).

Within the group of HPV-positive patients, ADC, f and D* × f values of PTs were significantly larger than those of LNs, while no systematic significant differences in diffusion parameters were reported within the HPV-negative patients (Table 3). Moreover, in HPV-positive patients significant correlations were found between PTs and LNs in both ADC and f values (correlation coefficient Rho = 0.486, p < 0.001 and Rho = 0.351, p = 0.020, respectively), while no relationship was found in HPV-negative patients.

The best predictive model for HPV positivity was obtained combining the alcohol intake and smoking habits (considered as categorical variables according to Table 1) with D_t values of PTs: the resultant accuracy was 80.8% [95%CI: 70.0%–89.1%] (sensitivity = 85.7% [95%CI: 73.8%–93.6%], specificity = 64.7% [95%CI: 38.4%–85.8%], PPV = 88.9% [95%CI: 80.6%–93.9%] and NPV = 57.9% [95%CI: 40.0%–74.1%]). The decision tree graph is illustrated in Supplementary Fig. 1. This predictive model was supported by the results obtained from univariate and multivariate logistic regression analyses, as indicated in Supplementary Table 3. Smoking status, alcohol intake, as well as ADC and D_t of PT were significant variables in the univariate analyses; due to the high collinearity between ADC and D_t, only D_t was included in the multivariate model, which suggested that both a reduced alcohol intake and a lower D_t of PT were associated with a greater risk of HPV positivity.

Three illustrative cases are presented in Figs. 1–3. Fig. 4 shows a direct comparison between DW-signal attenuation curves of Figs. 1 and 3, in PTs and LNs, separately.

4. Discussion

HPV-positive and HPV-negative OPSCCs have different carcinogenic mechanisms, genetic pathogenesis and prognoses [2–4,35]. A number of ongoing clinical trials are evaluating whether treatment intensity can be reduced in HPV-related OPSCCs, without jeopardizing clinical outcome [36]. Preliminary data are conflicting [37]; consistently, a subgroup of HPV-related OPSCC patients (up to 20%) still have a poor outcome after traditional approaches [35], suggesting that additional patient- and tumor-related factors are needed to better individualize treatment options beside HPV-status.

In this context, imaging biomarkers from multimodality techniques may help to achieve a more accurate patient stratification [38], as they can provide several quantitative indices related to tissue cellular density, tumor microenvironment, vascular perfusion and metabolism [9,7,11,12,17,39].

The ability of quantitative DWI (ADC) to differentiate HPV status in OPSCC had been already investigated in previous papers [9,11,12,17]. However, to our knowledge, only one investigation of Payudal et al. [39] used IVIM-DWI to characterize and monitor neck nodal metastases in HNSCCs during treatment, though a very small HPV-negative subgroup (n = 4) was included in this study. However, due to differences in the image acquisition protocol, particularly in the b-value range
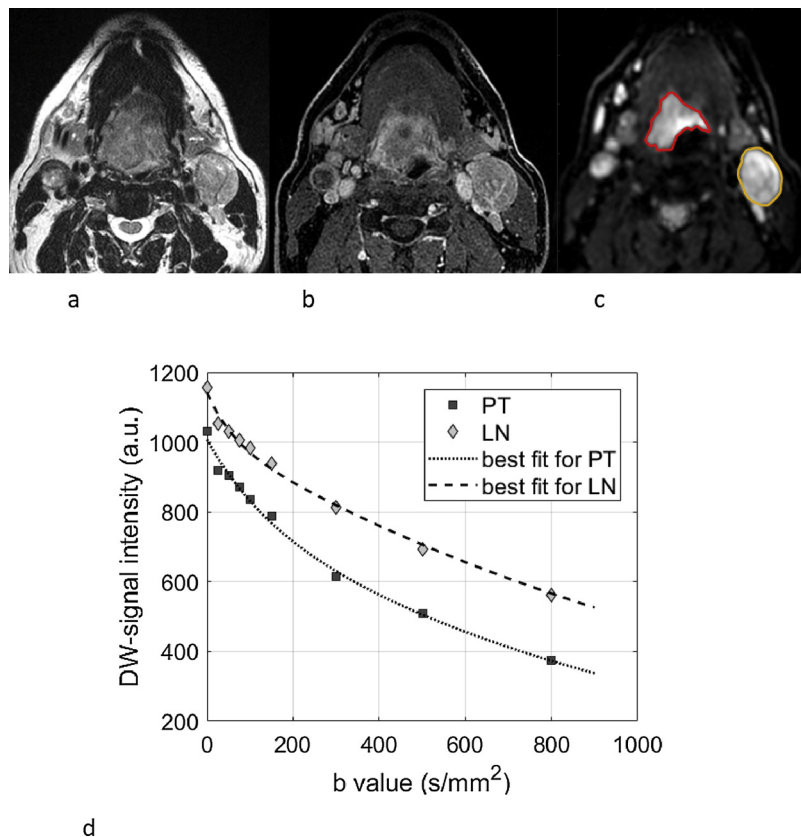
Table 3

Comparison between IVIM-DWI parameters of primary tumors (PTs) and the corresponding metastatic lymph nodes (LNs) according to the human papillomavirus (HPV) status.

Parameter*	HPV-negative (n = 14)			HPV-positive (n = 48)		
	PTs	LNs	p	PTs	LNs	p
ADC(10^{-3} mm^2/s)	1.51 (1.32-1.80)	1.31 (1.01-1.48)	0.056	1.28 (1.08-1.54)	1.14 (0.99-1.27)	**< 0.001**
D_t(10^{-3} mm^2/s)	1.24 (1.03-1.36)	1.01 (0.84-1.23)	0.245	0.97 (0.82-1.08)	0.91 (0.80-1.08)	0.422
f (%)	16.24 (9.32-28.85)	10.27 (7.50-15.79)	0.109	13.43 (10.39-19.44)	8.59 (7.01-11.70)	**< 0.001**
D*(10^{-3} mm^2/s)	16.11 (6.39-61.90)	17.68 (8.73-32.95)	0.917	18.94 (14.06-39.41)	19.59 (12.44-41.72)	0.514
D* × f (10^{-3} mm^2/s)	0.28 (0.13-0.48)	0.15 (0.08-0.31)	0.433	0.25 (0.18-0.50)	0.19 (0.10-0.31)	**0.002**

Median values (Interquartile range)*. P values refer to Wilcoxon test. Statistically significant p-values are bold. Abbreviations: ADC, apparent diffusion coefficient; D_t, tissue diffusion coefficient; D*, perfusion-related diffusion coefficient; f(%), perfusion fraction; D* × f, product of D* by f.

Fig. 1. 53-year-old non-smoker non-alcoholic man affected by HPV-positive oropharyngeal squamous cell carcinoma in the base of the tongue, with a large solid lymph-node in the left IIa level and a smaller metastatic lymph-node in the right IIa levels on T2-weighted image (a), post contrast LAVA image (b) and diffusion-weighted image obtained with $b = 800$ mm^2/s with the user-defined lesion contours (c). Both PT and LNs showed restricted water molecule mobility on diffusion-weighted image obtained with $b = 800$ mm^2/s. Curves of DW-signal attenuation in the primary tumor and the largest lymph-node, with the best bi-exponential fits (d). The ADC/D_t values was $1.377/0.991 \times 10^{-3}$ mm^2/s and $0.953/0.738 \times 10^{-3}$ mm^2/s for PT and the largest LN, respectively.

investigated, a direct comparison with our diffusion parameters of LNs was not possible. In accordance with previous investigations, we found that patients with HPV-related OPSCC smoked and drunk less [10,40,41] and were more likely to have a higher N-stage disease [8,11,15,35,41]. Even if they were younger compared with patients affected by non HPV-related OPSCCs [41], no statistically significant differences emerged in age. This may be due to the increased age of diagnosis for HPV-positive patients, as recently reported by Rettig et al. [42].

We found significantly lower values for both ADC and D_t of PTs in HPV-positive patients compared to HPV-negative patients consistently to earlier studies [10,12,13]. The difference in D_t of PTs between HPV-negative and HPV-positive patients was observed regardless of smoking and drinking habits, while only a trend towards significance in D_t emerged for LNs (Table 2). Our findings suggest that the perfusion-free diffusion coefficient, D_t, may better reflect HPV-related tumor differences, probably because it is more sensitive to the cellular microstructure, compared to ADC, in accordance with previous prognostic studies [25,29]

Even if no conclusive explanation has been provided to support differences in diffusion parameters by HPV status, Driessen et al. [12] speculated that it may be attributable to a smaller tumor-stroma component observed at pathology in HPV-positive OPSCC, which was found to be positively related to ADC [12]. Interestingly, Ward et al. [43] showed that the differences in ADC-values between HPV-positive and HPV-negative OPSCC might also reflect differences in tumor infiltrating lymphocytes: increased levels of lymphocytes were observed in HPV-positive patients, which may contribute to explain both the lower ADC values and the better survival of these patients.

Decreased ADCs in OPSCC with regional control after chemo-radiotherapy has been also attributed to a lesser amount of necrosis and hypoxia, which would negatively impact on the tumor response probability [44,45]. In this regard, we point out that we included the necrotic portion of the tumor in the analyses, considering that the present

investigation is part of a larger prospective study aimed at investigating the ability of IVIM-DWI to predict tumor response to chemo-radiotherapy.

However, concerning the perfusion-related parameters, we did not find any association between f, D^* and $D^* \times f$ and HPV status, suggesting that HPV-positive and HPV-negative OPSCCs have similar perfusion characteristics (Table 2), in agreement with other studies [18,46]. Moreover, cell line experiments and in vivo studies by PET-CT imaging indicated that the level of hypoxia was the same in HPV-positive and HPV-negative head and neck cancers [4].

It should be noted that f, D^* and $D^* \times f$ usually had a larger statistical dispersion, compared to ADC and D_t (Table 2), because the perfusion-related parameters are known to be more susceptible to poor SNR levels [23]. For this purpose, in order to obtain more reliable D^* and f values, we decided to perform the IVIM analyses on VOI-based measurements (rather than on single voxels).

Previous studies documented that, compared to HPV-negative, HPV-positive LNs were more cystic [19], however we did not find any significant difference in terms of LN morphology on the basis of the HPV status, probably because of the small number of cystic LNs in our patient population (n = 4).

Within the group of HPV-positive patients, LNs showed significantly lower ADC values, compared to ADC of corresponding PTs, which may be attributed to a lower perfusion level in LNs, as suggested by the significantly decreased f and $D^* \times f$ values (Table 3). Also Lu et al. [27] reported that PTs had significantly higher perfusion fraction f in comparison with LNs, which is in accordance with our data for HPV-positive patients, while we found only a trend toward significance in HPV-negative patients. They also documented a lower diffusion coefficient D_t in PTs, in disagreement with our findings.

More interestingly, significant correlations were found between ADC values of PTs and LNs, as well as between f values, while no relationship was found in HPV-negative patients. Even if we cannot exclude that this may be due to the smaller HPV-negative population, we
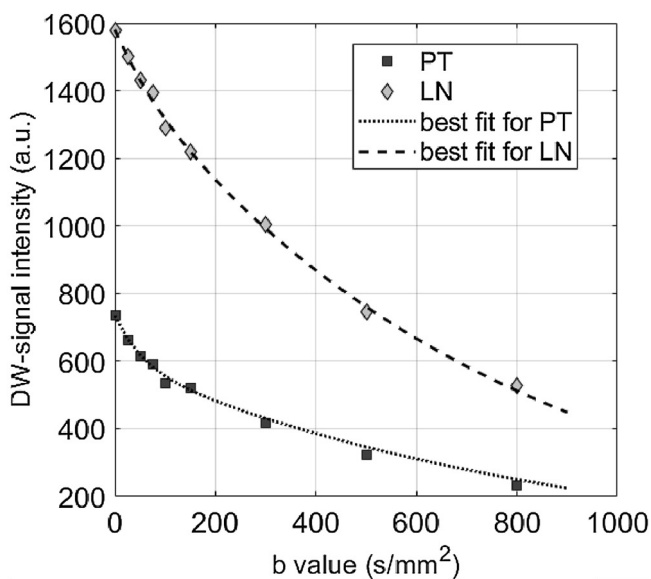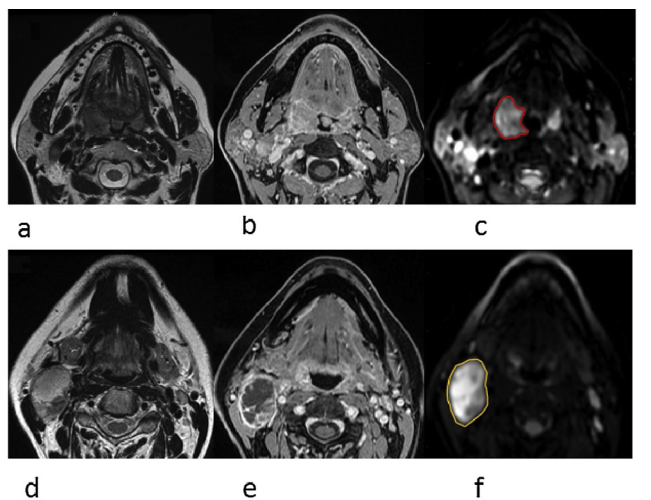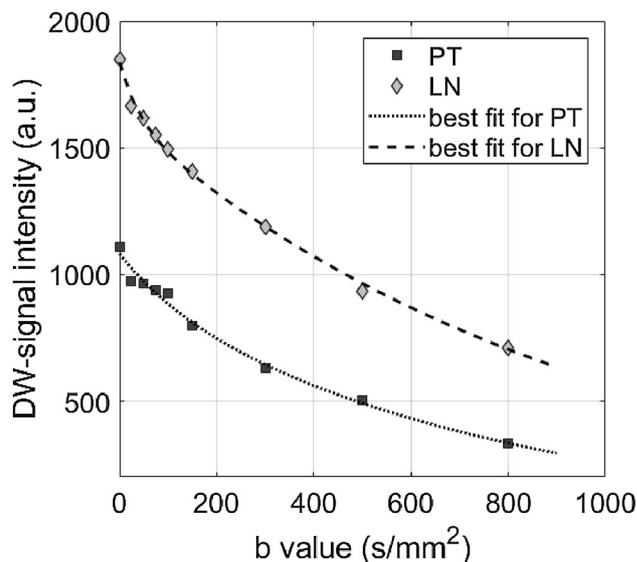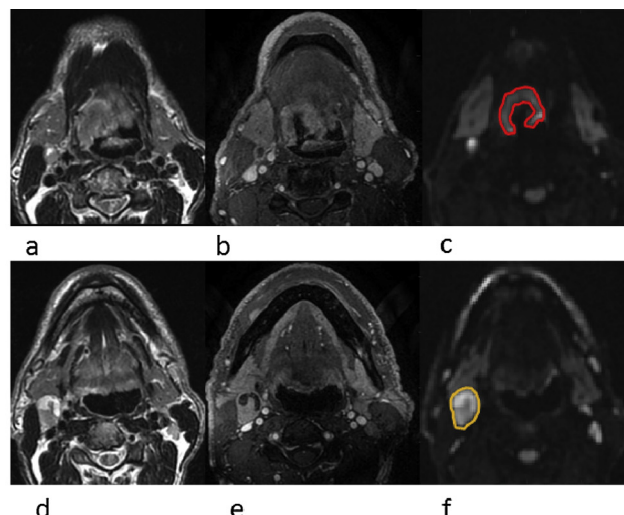
Fig. 2. 56-year-old non-smoker non-alcoholic woman affected by a HPV-positive oropharyngeal squamous cell carcinoma in the right palatine tonsil, with an almost completely cystic node in the right IIa level, on T2-weighted image (a,d), post contrast LAVA images (b,e) and diffusion-weighted image obtained with b = 800 mm²/s with the user-defined lesion contours (c,f). Curves of DW-signal attenuation in the primary tumor and the largest lymph-node, with the best bi-exponential fits (g). In PT, the large gap between ADC and D_t values (1.592 and 1.184 $\times 10^{-3}$ mm²/s, respectively) suggests a relevant perfusion contribution, as also indicated by the high values of f and D*$\times f$ (18.9% and 0.33 $\times 10^{-3}$ mm²/s, respectively) and by the initial shape of the signal attenuation curve. The high ADC and D_t values in LN (1.441 and 1.320 $\times 10^{-3}$ mm²/s, respectively) can be explained by the dominant fluid (avascular) component, in accordance with the low f and D*$\times f$ (6.9% and 0.09 $\times 10^{-3}$ mm²/s, respectively).

Fig. 3. 57-year-old man, heavy smoker and alcoholic, affected by HPV-negative oropharyngeal squamous cell carcinoma in the base of the tongue, with a partially necrotic lymph node in the right IIa level, on T2-weighted images (a,d), post contrast LAVA images (b,e) and diffusion-weighted images obtained with b = 800 mm²/s with the user-defined lesion contours (c,f). Curves of DW-signal attenuation in the primary tumor and the largest lymph-node, with the best bi-exponential fits (g). The ADC/D_t values in PT and LN were relatively high (1.598/1.265 $\times 10^{-3}$ mm²/s and 1.289/1.046 $\times 10^{-3}$ mm²/s, respectively), if compared to those observed in HPV-negative patients, as better illustrated in Fig. 4.

may hypothesize that the histological features of PT may influence those of metastatic LNs in HPV-positive patients. Similarly, Sharma et al. [15] found a significant concordance of SUVmax between PTs and respective LNs for HPV-positive patients, suggesting that HPV-related OPSCC may have a more homogeneous metabolic tumor phenotype, caused by a homogenously HPV triggered cancerogenesis.

Differently from other investigators [13], a model based on only ADC values of PTs and LNs did not provide a satisfactory prediction of HPV status in our patient population. However, by adding alcohol intake and smoking habits to D_t values of PTs, we could improve the

positive predictive value up to almost 90%. The potential of IVIM-DWI imaging, together with patient habits, to detect the HPV positivity, may have important clinical implications when the primary tumor is not easily accessible to biopsy (i.e. deep base of tongue tumors), when the patient refuses invasive procedures or when standard HPV testing provides conflicting results (i.e. discordance between HPV and p16 status).

This prospective study has some limitations. Our findings should be corroborated on a larger patient population, particularly the HPV-negative population has a small sample size, which reflects the increasing incidence rate of HPV-related OPSCC. Similarly, since PPV is strictly related to the prevalence of disease in the population, our results should be interpreted accordingly. Future investigations from this on-going
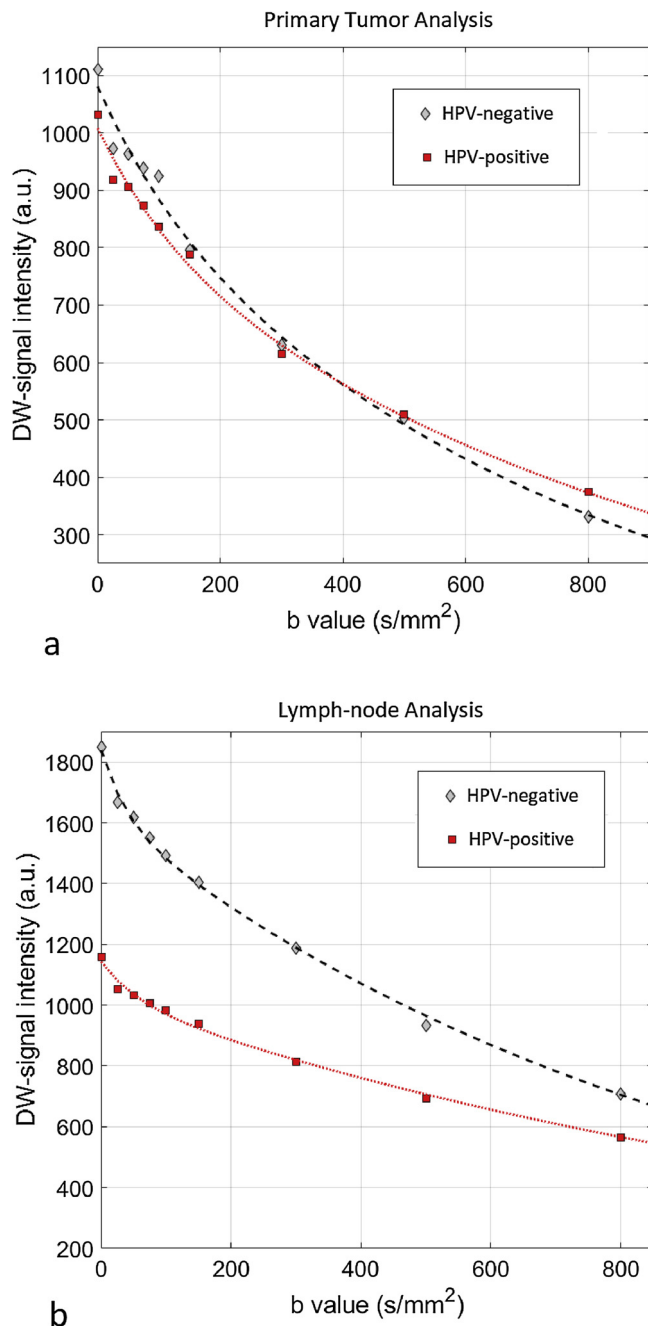
Fig. 4. Comparison between the DW-signal attenuation curves of the cases of Figs. 1 and 3, is proposed in PTs and LNs, showing a slower water molecule diffusivity (slower signal attenuation), both in the primary tumor and lymph-node for the HPV-positive patient, compared to the HPV-negative one.

study will include IVIM-DWI analysis also during radio-chemotherapy and follow up data, to investigate the ability of IVIM-DWI to predict tumor response to chemo-radiotherapy. This should help in risk stratifications of patients, according to both clinical and imaging characteristics, to better individualize treatment options especially for those HPV-positive patients having bad prognosis.

In conclusion, significant correlations were found between IVIM-DWI and HPV status in OPSCCs. Our findings suggest that the perfusion-free diffusion coefficient, D_t, may better reflect the HPV-related tumor differences, compared to conventional ADC. Whereas the perfusion-related parameters, f, D^* and $D^* \times f$ were not able to reliably discriminate HPV-positive from HPV-negative OPSCC.

Declaration of Competing Interest

None of the authors have potential conflict of interest including any financial, personal or other relationships with other people or organizations that could inappropriately influence this work.

Appendix A. Supplementary data

Supplementary material related to this article can be found, in the online version, at doi:https://doi.org/10.1016/j.ejrad.2019.08.009.

References

[1] M.B. Khalid, P. Ting, A. Pai, et al., Initial presentation of human papillomavirus-related head and neck cancer: a retrospective review, Laryngoscope (2018).
[2] N. Vigneswaran, M.D. Williams, Epidemiologic trends in head and neck cancer and aids in diagnosis, Oral Maxillofac. Surg. Clin. North Am. 26 (2) (2014) 123–141.
[3] J.M. Friedman, M.J. Stavas, A.J. Cmelak, Clinical and scientific impact of human papillomavirus on head and neck cancer, World J. Clin. Oncol. 5 (4) (2014) 781–791.
[4] L.G. Marcu, Future treatment directions for HPV-associated head and neck cancer based on radiobiological rationale and current clinical evidence, Crit. Rev. Oncol. Hematol. 103 (2016) 27–36.
[5] B. O'Sullivan, W.M. Lydiatt, B.H. Haughey, M. Brandwein-Gensler, C.M. Glastonbury, J.P. Shah, et al., HPV-mediated (p16+) oropharyngeal cancer, in: M.B. Amin, S. Edge, F. Greene (Eds.), AJCC Cancer Staging Manual, 8th ed., Springer, New York, 2017, pp. 113–121.
[6] S.C. Cantrell, B.W. Peck, G. Li, et al., Differences in imaging characteristics of HPV-positive and HPV-Negative oropharyngeal cancers: a blinded matched-pair analysis, Am. J. Neuroradiol. 34 (10) (2013) 2005–2009.
[7] K. Buch, A. Fujita, B. Li, et al., Using texture analysis to determine human papillomavirus status of oropharyngeal squamous cell carcinomas on CT, Am. J. Neuroradiol. 36 (7) (2015) 1343–1348.
[8] A. Fujita, K. Buch, M.T. Truong, et al., Imaging characteristics of metastatic nodes and outcomes by HPV status in head and neck cancers, Laryngoscope 126 (2) (2016) 392–398.
[9] A. Fujita, K. Buch, B. Li, et al., Difference between HPV-Positive and HPV-Negative non-oropharyngeal head and neck Cancer: texture analysis features on CT, J. Comput. Assist. Tomogr. 40 (1) (2016) 43–47.
[10] M. Nakahira, N. Saito, H. Yamaguchi, et al., Use of quantitative diffusion-weighted magnetic resonance imaging to predict human papilloma virus status in patients with oropharyngeal squamous cell carcinoma, Eur. Arch. Otorhinolaryngol. 271 (5) (2014) 1219–1225.
[11] C.S. Schouten, P. de Graaf, E. Bloemena, et al., Quantitative diffusion-weighted MRI parameters and human papillomavirus status in oropharyngeal squamous cell carcinoma, Am. J. Neuroradiol. 36 (4) (2015) 763–767.
[12] J.P. Driessen, A.J. van Bemmel, P.M. van Kempen, et al., Correlation of human papillomavirus status with apparent diffusion coefficient of diffusion-weighted MRI in head and neck squamous cell carcinomas, Head Neck 38 (Suppl 1) (2016) E613–618.
[13] M.W. Chan, K. Higgins, D. Enepekides, et al., Radiologic differences between human papillomavirus-related and human papillomavirus-unrelated oropharyngeal carcinoma on diffusion-weighted imaging, J. Otorhinolaryngol. Relat. Spec. 78 (6) (2016) 344–352.
[14] Y.S. Choi, M. Park, H.J. Kwon, et al., Human papillomavirus and epidermal growth factor receptor in oral cavity and oropharyngeal squamous cell carcinoma: correlation with dynamic contrast-enhanced MRI parameters, Am. J. Roentgenol. 206 (2) (2016) 408–413.
[15] S.J. Sharma, C. Wittekindt, J. Knuth, et al., Intraindividual homogeneity of (18)F-FDG PET/CT parameters in HPV-positive OPSCC, Oral Oncol. 73 (2017) 166–171.
[16] E. Mena, M. Taghipour, S. Sheikhbahaei, et al., Value of intratumoral metabolic heterogeneity and quantitative 18F-FDG PET/CT parameters to predict prognosis in patients with HPV-Positive primary oropharyngeal squamous cell carcinoma, Clin. Nucl. Med. 42 (5) (2017) e227–e234.
[17] D. Aramburu Nunez, A. Lopez Medina, M. Mera Iglesias, et al., Multimodality functional imaging using DW-MRI and (18)F-FDG-PET/CT during radiation therapy for human papillomavirus negative head and neck squamous cell carcinoma: meixoeiro Hospital of Vigo Experience, World J. Radiol. 9 (1) (2017) 17–26.
[18] M. Han, S.J. Lee, D. Lee, et al., Correlation of human papilloma virus status with quantitative perfusion/diffusion/metabolic imaging parameters in the oral cavity and oropharyngeal squamous cell carcinoma: comparison of primary tumor sites and metastatic lymph nodes, Clin. Radiol. 73 (8) (2018) 757.e21–757.e27.
[19] M.W. Chan, E. Yu, E. Bartlett, et al., Morphologic and topographic radiologic features of human papillomavirus-related and -unrelated oropharyngeal carcinoma, Head Neck 39 (8) (2017) 1524–1534.

[20] S. Kim, L. Loevner, H. Quon, et al., Diffusion-weighted magnetic resonance imaging for predicting and detecting early response to chemoradiation therapy of squamous cell carcinomas of the head and neck, Clin. Cancer Res. 15 (3) (2009) 986–994.

[21] A. Srinivasan, T.L. Chenevert, B.A. Dwamena, et al., Utility of pretreatment mean apparent diffusion coefficient and apparent diffusion coefficient histograms in prediction of outcome to chemoradiation in head and neck squamous cell carcinoma, J. Comput. Assist. Tomogr. 36 (1) (2012) 131–137.

[22] S. Chawla, S. Kim, L. Dougherty, et al., Pretreatment diffusion-weighted and dynamic contrast-enhanced MRI for prediction of local treatment response in squamous cell carcinomas of the head and neck, Am J Roentgenol. 200 (1) (2013) 35–43.

[23] C. Federau, Intravoxel incoherent motion MRI as a means to measure in vivo perfusion: a review of the evidence, NMR Biomed. 30 (11) (2017).

[24] D. Le Bihan, E. Breton, D. Lallemand, et al., Separation of diffusion and perfusion in intravoxel incoherent motion MR imaging, Radiology 168 (1988) 497–505.

[25] D.P. Noij, R.M. Martens, J.T. Marcus, et al., Intravoxel incoherent motion magnetic resonance imaging in head and neck cancer: a systematic review of the diagnostic and prognostic value, Oral Oncol. 68 (2017) 81–91.

[26] L. Liang, X. Luo, Z. Lian, et al., Lymph node metastasis in head and neck squamous carcinoma: efficacy of intravoxel incoherent motion magnetic resonance imaging for the differential diagnosis, Eur. J. Radiol. 90 (2017) 159–165.

[27] Y. Lu, J.F. Jansen, H.E. Stambuk, et al., Comparing primary tumors and metastatic nodes in head and neck cancer using intravoxel incoherent motion imaging: a preliminary experience, J. Comput. Assist. Tomogr. 37 (3) (2013) 346–352.

[28] T. Hauser, M. Essig, A. Jensen, et al., Prediction of treatment response in head and neck carcinomas using IVIM-DWI: evaluation of lymph node metastasis, Eur. J. Radiol. 83 (5) (2014) 783–787.

[29] S. Marzi, F. Piludu, G. Sanguineti, et al., The prediction of the treatment response of cervical nodes using intravoxel incoherent motion diffusion-weighted imaging, Eur. J. Radiol. 92 (2017) 93–102.

[30] M. Mena, M. Taberna, S. Tous, et al., Double positivity for HPV-DNA/p16ink4a is the biomarker with strongest diagnostic accuracy and prognostic value for human papillomavirus related oropharyngeal cancer patients, Oral Oncol. 78 (2018) 137–144.

[31] G. Sanguineti, F. Ricchetti, B. Wu, et al., Volumetric change of human papillomavirus-related neck lymph nodes before, during, and shortly after intensity-modulated radiation therapy, Head Neck 34 (11) (2012) 1640–1647.

[32] R.H. Byrd, J.C. Gilbert, J. Nocedal, A trust region method based on interior point techniques for nonlinear programming, Math. Program. 89 (2000) 149–185.

[33] D. Le Bihan, R. Turner, The capillary network: a link between IVIM and classical perfusion, Magn. Reson. Med. 27 (1992) 171–178.

[34] L. Breiman, J.H. Friedman, R.A. Olshen, et al., Classification and Regression Trees, Chapman & Hall, Boca Raton, FL, 1984.

[35] C. Liu, G. Talmor, G.M. Low, et al., How does smoking change the clinicopathological characteristics of human papillomavirus-positive oropharyngeal squamous cell carcinoma? One medical center experience, Clin. Med. Insights Ear Nose Throat 19 (11) (2018) 1–6.

[36] H. Mirghani, P. Blanchard, Treatment de-escalation for HPV-driven oropharyngeal cancer: where do we stand? Clin. Transl. Radiat. Oncol. 8 (2017) 4–11.

[37] H. Mehanna, M. Robinson, A. Hartley, et al., Radiotherapy plus cisplatin or cetuximab in low-risk human papillomavirus-positive oropharyngeal cancer (De-ESCALaTE HPV): an open-label randomised controlled phase 3 trial, Lancet (2018), https://doi.org/10.1016/S0140-6736(18)32752-1.

[38] J. Caudell, J.F. Torres-Roca, R.J. Gillies, et al., The future of personalised radiotherapy for head and neck cancer, Lancet Oncol. 18 (2017) e266–e273.

[39] R. Paudyal, J.H. Oh, N. Riaz, et al., Intravoxel incoherent motion diffusion-weighted MRI during chemoradiation therapy to characterize and monitor treatment response in human papillomavirus head and neck squamous cell carcinoma, J. Magn. Reson. Imaging 45 (4) (2017) 1013–1023.

[40] S.H. Huang, B. Perez-Ordonez, F.F. Liu, et al., Atypical clinical behavior of p16-confirmed HPV-related oropharyngeal squamous cell carcinoma treated with radical radiotherapy, Int. J. Radiat. Oncol. Biol. Phys. 82 (1) (2012) 276–283.

[41] M. Taberna, M. Mena, M.A. Pavon, et al., Human papillomavirus-related oropharyngeal cancer, Ann. Oncol. 28 (10) (2017) 2386–2398.

[42] E.M. Rettig, M. Zaidi, F. Faraji, et al., Oropharyngeal cancer is no longer a disease of younger patients and the prognostic advantage of Human Papillomavirus is attenuated among older patients: analysis of the National Cancer database, Oral Oncol. 83 (2018) 147–153.

[43] M.J. Ward, S.M. Thirdborough, T. Mellows, et al., Tumor-infiltrating lymphocytes predict for outcome in HPV-positive oropharyngeal cancer, Br. J. Cancer 110 (2) (2014) 489–500.

[44] A.D. King, K.K. Chow, K.H. Yu, et al., Head and neck squamous cell carcinoma: diagnostic performance of diffusion-weighted MR imaging for the prediction of treatment response, Radiology 266 (2) (2013) 531–538.

[45] M. Lambrecht, B. Van Calster, V. Vandecaveye, et al., Integrating pretreatment diffusion weighted MRI into a multivariable prognostic model for head and neck squamous cell carcinoma, Radiother. Oncol. 110 (3) (2014) 429–434.

[46] J.F. Jansen, D.L. Carlson, Y. Lu, et al., Correlation of a priori DCE-MRI and (1)H-MRS data with molecular markers in neck nodal metastases: initial analysis, Oral Oncol. 48 (8) (2012) 717–722.